Global and Planetary Change 243 (2024) 104628

Contents lists available at ScienceDirect

Global and Planetary Change

journal homepage: www.elsevier.com/locate/gloplacha

Research Article

Concurrent trend turnings of drought severity across Afro-Eurasian continent since 1950

Wei Lou [a], Cheng Sun [a,*], Bin Zuo [b]

[a] State Key Laboratory of Remote Sensing Science, Faculty of Geographical Science, Beijing Normal University, Beijing 100875, China
[b] PLA Dalian Naval Academy, Dalian 116018, China

ARTICLE INFO

Editor: Storelvmo Trude

Keywords:
Frequency of drought trend turnings
Drought in Afro-Eurasian
Running Slope Difference *t*-test

ABSTRACT

Rapidly intensifying global land drought poses severe threats to human societies, economies, and ecosystems. While previous studies have primarily investigated long-term drought trends, the frequency and concurrence of trend turnings have been largely neglected. In this study, we address this gap by employing the Running Slope Difference (RSD)-*t*-test to quantify trend turning frequency in Afro-Eurasian drought severity. Based on Palmer Drought Severity Index (PDSI), our analysis indicates that the PDSI trend in most parts of the Afro-Eurasian continent has experienced two turnings since 1950, although, the types of trend turnings vary regionally. The concurrence of these PDSI trending turnings is further investigated. Around 1985, a dipole pattern emerged - Eastern Europe experiences a drying trend turning, accompanied by decreased P-E and intensified drought, while Sahel exhibits a wetting trend turning, with increased P-E and mitigated drought. Around 2000, a tripole pattern is observed in Eastern Eurasia: The Russian Far East and South Asia experienced a drying trend turning, with reduced P-E and intensified drought, while Northeast Asia exhibited a further wetting trend, characterized by increased P-E and mitigated drought. We further investigate the influence of large-scale circulation changes. The enhanced Northern Hemisphere warming trend before and after 1985 contributes to increased land surface high pressure and an amplified meridional temperature gradient, favoring cross-equatorial water vapor transport. This mechanism potentially drives the dipole pattern of trend turning observed around 1985. Additionally, the North Pacific Ocean Sea Surface Temperature (SST) exhibited an enhanced North Pacific Gyre Oscillation (NPGO) pattern around 2000, which induced a tripole atmospheric circulation pattern over East Asia, corresponding to the observed tripole pattern of PDSI trend turnings. The identified dipole and tripole patterns of drought trend turnings, and their potential links to large-scale atmospheric circulation changes, provide insights into the complex dynamics of land drought variability across Afro-Eurasian.

1. Introduction

Recent observations indicate an increasing trend in drought across most of the Northern Hemisphere's land areas (Dai, 2011; Nasrollahi et al., 2015). Meteorological droughts in regions such as West Africa, East Asia, South Asia and the Mediterranean have become more frequent, prolonged, and intense. This is evidenced by positive trends in their frequency, duration, and severity (Saleem et al., 2021; Spinoni et al., 2014). This intensification, driven by global temperature rise, has caused substantial losses in agriculture and socio-economic systems, particularly in arid and semi-arid regions (Ault, 2020; Leng and Hall, 2019; Overpeck, 2013; Vogel et al., 2019; Zeng et al., 2023). For instance, recent droughts in India and Pakistan have critically affected agricultural production and water resources, leading to decreased crop yields and heightened food insecurity (Chen et al., 2012; Sharma and Mujumdar, 2017; Ullah et al., 2023b; Xu et al., 2024). In the United States, droughts have reduced crop yields and increased wildfires, causing significant economic losses (Leeper et al., 2022; Motha, 2011). The population exposures to the extreme droughts in China and Pakistan are projected to increase (Chen and Sun, 2019; Chen et al., 2018; Saleem et al., 2023). Furthermore, prolonged droughts in regions like the Sahel and East Africa have had devastating and complex impacts on local ecosystems (Gebremeskel Haile et al., 2019; Simpkins, 2018). Hence, it is crucial to gain a comprehensive understanding of the evolving trends and spatial characteristics of droughts in major regions globally to develop effective drought prevention measures.

* Corresponding author.
E-mail address: scheng@bnu.edu.cn (C. Sun).

https://doi.org/10.1016/j.gloplacha.2024.104628
Received 16 March 2024; Received in revised form 24 September 2024; Accepted 4 November 2024
Available online 5 November 2024

Drought primarily results from sustained precipitation deficits or excessive evaporation. In mid-high latitude regions of Eurasia, drought intensification is mainly driven by temperature-induced evaporation increases (Sun et al., 2021). Conversely, in Africa, Southeast Asia, and eastern Australia, decreased precipitation is the primary cause (Ayugi et al., 2022; King et al., 2020; Phan-Van et al., 2022). Atmospheric/oceanic circulation anomalies strongly influence the regional drought conditions. El Niño-Southern Oscillation (ENSO) impacts droughts in North America and Eastern China (Singh et al., 2022). The North Atlantic Oscillation (NAO) contributes to droughts in northern China (Du et al., 2020). Severe droughts in eastern China are linked to weakening summer monsoons and the westward displacement of the Western Pacific Subtropical High (Chen et al., 2023; Liu et al., 2023). Long-term sea surface temperature (SST) trends and decadal oscillations, such as the Atlantic Multidecadal Oscillation (AMO) and the Pacific Decadal Oscillation (PDO), also influence regional droughts (Méndez and Magaña, 2010). The Sahel drought is affected by tropical Atlantic SST changes, the southward shift of the Inter-Tropical Convergence Zone (ITCZ), and the warming Indian Ocean's impact on anticyclonic circulation (Hagos and Cook, 2008). Additionally, anthropogenic greenhouse gas emissions and sulfate aerosols significantly impact global drought trends (Burke et al., 2006; Chiang et al., 2021). Global warming increases atmospheric water content and transport. This exacerbates drought in dry areas and intensifies wet conditions in wet areas (Byrne and O'Gorman, 2015). Reflective aerosol forcing enhances the SST gradient, triggering severe drying in the northern edge of the Atlantic ITCZ and the Sahel region (Biasutti and Giannini, 2006).

Under the combined influence of internal climate variability and external forcing, drought may exhibit non-stationary changes and drought trends may undergo multiple trend turnings. Previous research has predominantly concentrated on the long-term trends of individual drought time series and the linkages between drought concurrences in different regions (Dai, 2011; Dai, 2013; Herrera-Estrada et al., 2017; Mondal et al., 2023; Singh et al., 2021). Long-term linear trends may mask underlying non-linearities, such as opposing trends or turning points, within the original time series data. These non-linearities can be crucial for understanding the dynamics of specific systems. Presently, research on trend turnings primarily employs methods such as optimal piecewise linear regression (OPLR) (Tomé and Miranda, 2004) or running trend test (RTT) (Thanasis et al., 2011) to detect changes in climate variables such as air temperatures. Other studies employ the Ensemble Empirical Mode Decomposition method to identify secular trend in global drought, revealing the shifts of trend and nonlinear property of the secular trend (Leeper et al., 2022; Song et al., 2020). However, a comprehensive analysis of the frequency of significant shifts in global drought trends remains lacking. Furthermore, the internal linkages between drought trend turnings across different regions remains poorly investigated. Therefore, further research is warranted to investigate the frequency and spatiotemporal distribution of drought trend turnings, as well as the linkages between these turnings across diverse regions.

Recent decades have witnessed an alarming escalation in the frequency, duration, and intensity of droughts across numerous Afro-Eurasian regions, posing a formidable threat to sustainable development and human well-being (Balting et al., 2021; Mukherjee and Mishra, 2021). Elucidating the spatiotemporal patterns and drivers of drought trend turnings in Afro-Eurasian is crucial for developing effective mitigation and adaptation strategies. This study applies the Running Slope Difference (RSD) *t*-test (Zuo et al., 2019), a recently proposed method for detecting climate multiple trend turnings effectively. We use this method on Palmer Drought Severity Index (PDSI) data in Afro-Eurasian, aiming to identify the types, frequencies, and spatiotemporal distributions of trend turnings in drought severity. Through this analysis, we hope to gain deeper insight into the spatiotemporal patterns of drought in Afro-Eurasian, ultimately contributing to sustainable water resource management and socioeconomic development across Afro-Eurasian.

2. Data and methods

2.1. Data

In this study, we use the global monthly self-calibrating_PDSI dataset from UCAR (University Corporation for Atmospheric Research) (Dai, 2017). This dataset incorporates Penman-Monteith potential evapotranspiration and numerous forcing data sources, with a spatial resolution of 2.5° × 2.5°. The PDSI is more suitable for measuring drought over longer time scales, typically ranging from 9 to 18 months, effectively reflecting interannual variations in regional drought conditions (Guttman, 1998; Vicente-Serrano et al., 2010; Zhao et al., 2017). The PDSI data for the period 1950–2018 are selected and can be downloaded from the following website: http://www.cgd.ucar.edu/cas/catalog/climind/pdsi.html. The Standardized Precipitation–Evapotranspiration Index (SPEI) dataset is also used in this study for comparison, which has a spatial resolution of 0.5° × 0.5° and a monthly temporal resolution (Beguería et al., 2023). The SPEI is a multiscale index. To match the time scale of the PDSI, we used the SPEI-12, which represents annual variations in wet and dry conditions (Cao et al., 2022; Chen et al., 2022). The data can be downloaded from the following website: //spei.csic.es/database.html. This study employs both PDSI and SPEI to investigate drought trend changes. This multi-index approach enhances the robustness of our results by incorporating the strengths of each index.

To investigate the potential influence of large-scale atmospheric and oceanic circulation patterns on drought trends, we incorporate two climate indices into our analysis: the ENSO index and the North Pacific Gyre Oscillation (NPGO) index. The Niño3.4 index, the most commonly used index to represent ENSO intensity, is defined as the average of SST anomalies over the Niño3.4 region (5°S–5°N, 170°W–120°W). The NPGO index (Di Lorenzo et al., 2008) is defined as the time coefficient of the second empirical orthogonal function (EOF) of detrended sea surface height anomalies in the northeastern Pacific region. The NPGO index data can be downloaded from the following website: http://www.o3d.org/npgo/data/NPGO.txt. Monthly surface precipitation and potential evapotranspiration data are obtained from the Climatic Research Unit (CRU) gridded time series dataset, with a spatial resolution of 0.5° × 0.5°. The data can be downloaded from the following website: https://crudata.uea.ac.uk/cru/data/hrg/. Atmospheric circulation reanalysis data, including geopotential height, wind, and surface temperature, were obtained from the ERA5 surface reanalysis dataset. ERA5 is the fifth-generation global weather reanalysis product released by the European Centre for Medium-Range Weather Forecasts (ECMWF). The dataset covers the period 1950–2019, with a monthly temporal resolution and a spatial resolution of 0.25° × 0.25°. The data can be downloaded from the following website: //www.ecmwf.int/en/forecasts/datasets/reanalysis-datasets/era5. SST data is obtained from the HadiSST dataset, with a spatial resolution of 1° × 1°.

2.2. Running slope difference t-test

The RSD t-test is proposed by Zuo, which leverages the statistical significance of sub-sample trend slope differences (Zuo et al., 2020; Zuo et al., 2019). This recently proposed method is different from the previous methods such as OPLR and RTT, which can not distinguish between substantial turnings where the direction of the trend (positive or negative) remains consistent on both sides of the turning point (a type of turning between two significant same-sign trends of different magnitude). Specifically, the RTT method can only identify two scenarios: (1) a sign reversal, where a significant positive trend turnings to a significant negative trend (or vice versa), and (2) a trend-to-no-trend shift, where a significant linear trend becomes insignificant (or vice versa). The RSD t-test is an effective data-driven tool for detecting trend turnings in time series, with three major advantages: ability to detect

Table 1
Types of trends turning.

Trend Turning Type	Number	Wet/ Dry	Trend Before Turning	Trend After Turning
Wetting (Previous trend significantly lower than subsequent trend)	1	Wetting	Significant Drying (−)	No trend change (0)
	2	Wetting	No trend change (0)	Significant Wetting (+)
	3	Wetting	Significant Drying (−)	Significant Wetting (+)
	4	Wetting	Significant Wetting (+)	Significant Wetter (++)
	5	Wetting	Significant Drier (−-)	Significant Drying (−)
Drying (Previous trend significantly higher than subsequent trend)	6	Drying	Significant Wetting (+)	No trend change (0)
	7	Drying	No trend change (0)	Significant Drying (−)
	8	Drying	Significant Wetting (+)	Significant Drying (−)
	9	Drying	Significant Wetter (++)	Significant Wetting (+)
	10	Drying	Significant Drying (−)	Significant Drier (−-)

Notes: +, −, and 0 represent significant positive, significant negative, and no significant trends, respectively; ++ represents positive trends with larger trend values; −- represents negative trends with smaller trend values.

multiple turning-points, capacity to detect all three types of trend turnings, and great performance of avoiding false alarm.

The differential nature of trends between preceding and succeeding phases represents a fundamental characteristic of trend turnings. To identify inflection points, the RSD t-test employs a statistical t-test based on the discrepancies in slopes. The essence of this methodology lies in the construction of a trend differential statistic that adheres to a t-distribution. Let Y: $\{y_i = \beta_Y i+\alpha_Y+\varepsilon_i | 1 \le i \le n\}$ and Z: $\{z_j = \beta_Z j+\alpha_Z+\varepsilon_j | 1 \le j \le m\}$ be two sample sub-series. Assume that the error terms ε_i and ε_j are normally distributed independent random variables with zero mean and same variance σ^2. The form of this statistical t-test for slope differences is as follows:

$$t_{slope} = \frac{\sqrt{C}(\widehat{\beta_Y} - \widehat{\beta_Z})}{\sqrt{\frac{\left(\sum_{i=1}^{n}(y_i-\widehat{y_i})^2+\sum_{j=1}^{m}(z_j-\widehat{z_j})^2\right)}{n+m-4}}} \quad (1)$$

$$C = \frac{NM}{N+M} \quad (2)$$

where $\widehat{\beta_Y}$ and $\widehat{\beta_Z}$ are the least squares linear slope of Y and Z, respectively, $\widehat{y_i}$ and $\widehat{z_j}$ are the least squares regressions of y_i and z_j, respectively, $N = \sum_{i=1}^{n}\left(i - \frac{n+1}{2}\right)^2$ and $M = \sum_{j=1}^{n}\left(j - \frac{m+1}{2}\right)^2$ are two known constants of n and m, respectively. The null hypothesis of no slope difference between Y and Z is rejected at the significance level α if $|t_{slope}| \ge t_f, 1-\alpha/2$, where $f = n+m-4$ is the degrees of freedom of the statistic t_{slope}.

If the above Y and Z are two adjacent sub-series of the sample time series, then we can use the statistic t_{slope} to detect whether there is a trend turn between Y and Z. This study identify trend turning in PDSI by comparing the trends of the previous and subsequent sequences (as shown in Table 1). Let L be the sample time series and τ be the chosen sliding window. The trend turning point of L is identified from the slope difference between the sub-series (for a length of sliding window τ) before and after each point using the t_{slope} test. The calculation formula for the effective degrees of freedom N^{eff} is as follows:

$$\frac{1}{N^{eff}} \approx \frac{1}{N} + \frac{2}{N}\sum_{j=1}^{N}\frac{N-j}{N}\rho_{XX}(j)\rho_{YY}(j) \quad (3)$$

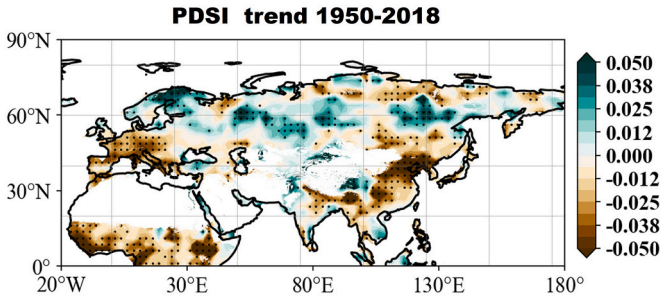

Fig. 1. Spatial distribution of PDSI trends in Afro-Eurasian during 1950–2018 (yr^{-1}). Areas significant at the 95 % confidence level are denoted by dots.

where N is the sample size, $\rho_{XX}(j)$is the autocorrelation of the series X at the time of sampling, $\rho_{YY}(j)$ is for the series Y, and j is the time lag.

The RSD t-test employs a two-stage process to detect trend turnings. Initially, a sliding detection process is employed to identify potential trend turning points, followed by a subsequent examination process to confirm the presence of trend inflection points. In this study, when conducting the detection of PDSI sequences for each grid point, the primary detection parameters for the RSD t-test method are set as follows: For the trend turning detection time scale parameter T, we adopt a setting of 15 years consistent with Karl's findings(Karl et al., 2000). The sliding window for detection is set as τ = T-1. To enhance sensitivity and avoid overlooking potential trend turning points, the confidence level threshold is set at 90 %. A 90 % confidence level provides sufficient sensitivity and accuracy in detecting trend turning points, maintaining high credibility in practical applications. A preprocessing step involving a 7-year sliding average is applied to the drought index sequences for each grid point to improve the accuracy of the detection process. We also conduct the analysis at a 95 % confidence level. The results remain consistent at both confidence levels. This consistency strengthens the robustness of our findings detected at the 90 % confidence level. Additionality, we analyze the causes of the shift in drought trends attributed to atmospheric circulation by examining the differences in atmospheric circulation patterns before and after the drought trend turning point. The time period for analyzing atmospheric circulation trends aligns with the period for drought analysis, and the significance testing method employed is consistent with the RSD-t-test.

2.3. Definition of trend turning types

When analyzing long time series, two adjacent periods may display significantly different trends, referred to as trend turnings. The drought trend turnings can be categorized into two types: wetting trend turnings and drying trend turnings. Turning types where the trend before the turning is significantly smaller than the trend after the turning is defined as wetting trend turnings. Turning types where the trend before the turning is significantly larger than the trend after the turning is defined as drying trend turnings. Based on the different combinations of pre-turning and post-turning trends, the specific types of wetting and drying trend turnings are shown in Table 1.

3. Results

3.1. Spatiotemporal distribution of trend turnings frequency in Afro-Eurasian drought severity

3.1.1. Long-term trend of Afro-Eurasian PDSI

The PDSI is one of the most widely used drought indices. It takes into account the balance of precipitation, runoff, and evapotranspiration, and can effectively characterize drought severity (Han and Singh, 2023). As shown in Fig. 1, the long-term trend of the PDSI time series from 1950 to 2018 in Afro-Eurasian reveals intensifying drought (decreasing PDSI),

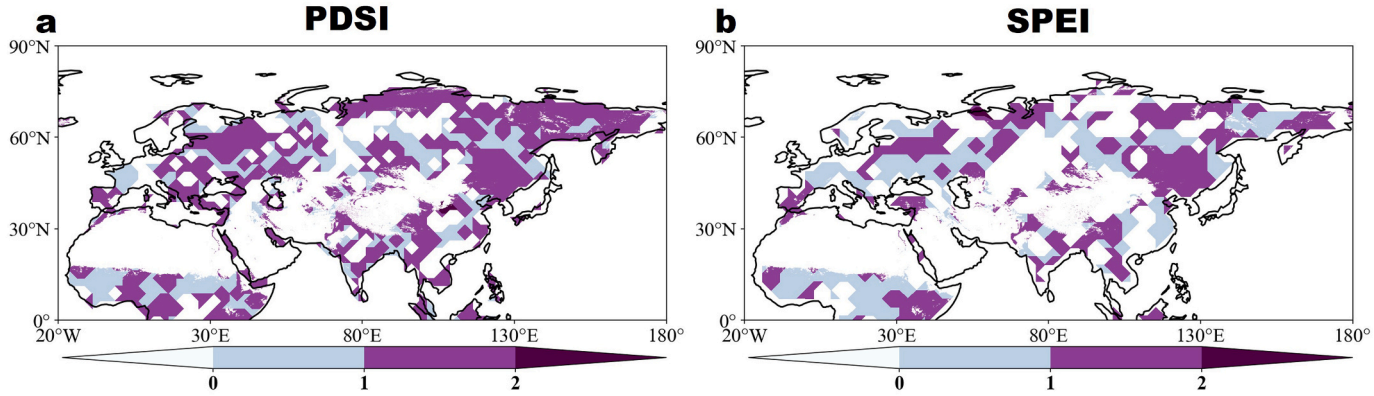

Fig. 2. Spatial distribution of the total frequencies of trend turnings of (a) PDSI (b) SPEI in Afro-Eurasian during 1950–2018.

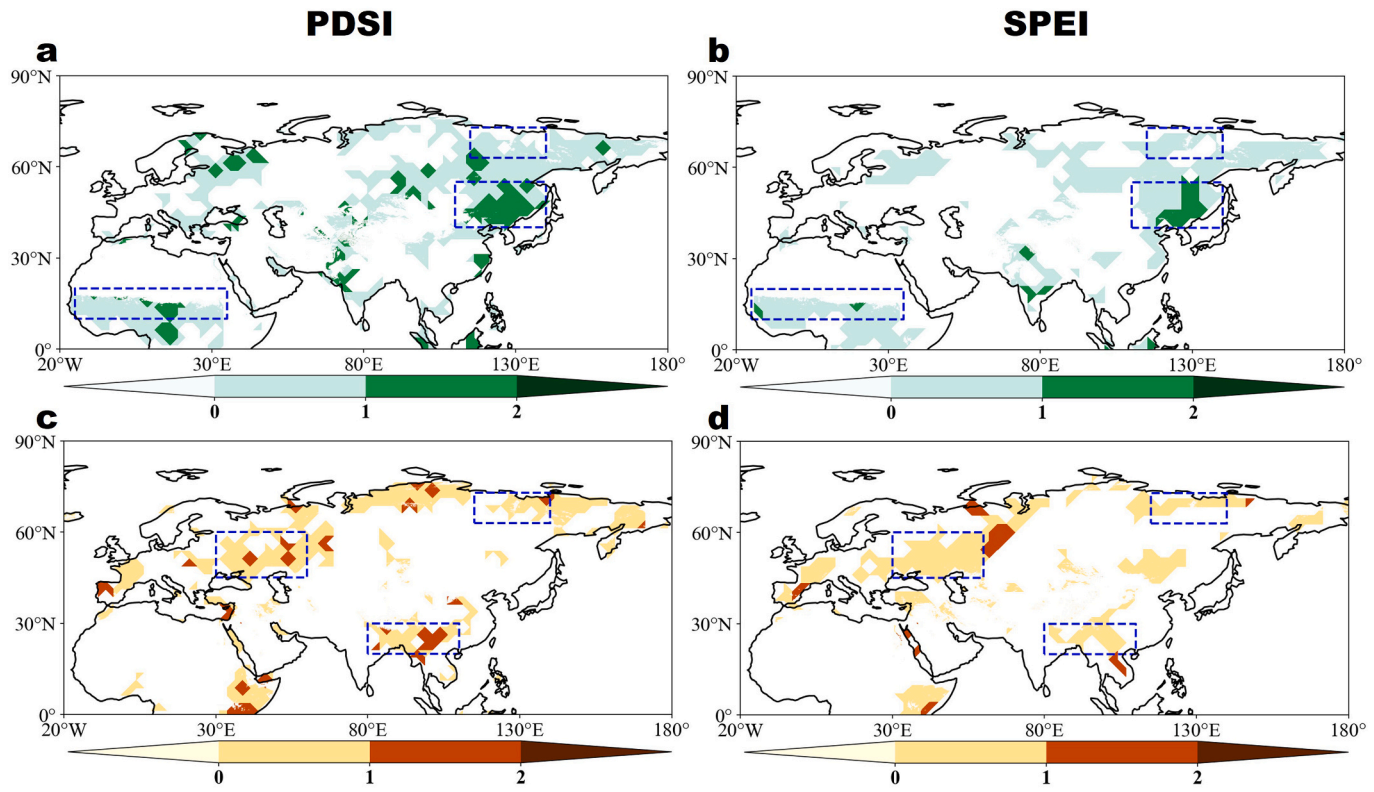

Fig. 3. Frequency (a) of PDSI (b) SPEI wetting trend turnings during 1950–2018. Frequency (c) of PDSI (d) SPEI drying trend turnings in Afro-Eurasian during 1950–2018. The blue box in it is the defined the region of Eastern Europe (45°N ~ 60°N, 30°E ~ 60°E), Sahel (10°N ~ 20°N, 15° W ~ 30°E), Russian Far East (63°N ~ 73°N, 115°E ~ 140°E), Northeast Asia (40°N ~ 55°N, 110°E ~ 140°E), and South Asia (20°N ~ 30°N, 80° W ~ 110°E). (For interpretation of the references to colour in this figure legend, the reader is referred to the web version of this article.)

especially in regions like East Asia, Western Europe, and African Sahel. Conversely, some mid- and high-latitude regions exhibit a wetting trend (increasing PDSI). SPEI has also been used extensively to assess drought severity, as shown in Fig. S1, again calculating long-term trends, with results largely consistent with the PDSI. Notably, droughts are influenced by both external forcing and internal climate variability, leading to non-stationary trends and multiple turning points. Previous research has indicated that drought shows distinct non-stationary characteristics in inland arid areas during 1962–2015 (He et al., 2021). In Oman, drought conditions have worsened over recent decades, with a significant turning point around 1997/1998 (El Kenawy et al., 2020). Likewise, a significant shift in drought patterns occurred across all regions of China around 1970, with a 2–8-year significant period (Wang et al., 2017). Analyzing long-term PDSI time series solely through linear trends risks obscuring opposing trends or turning points, potentially crucial for specific regional ecosystems. To comprehensively understand the trend changes of drought severity, it is necessary to calculate the inter-decadal trend turning frequency in the PDSI time series for each grid point in Africa-Eurasian.

3.1.2. *Spatial distribution of Afro-Eurasian PDSI trend turning frequency*

The results of the RSD *t*-test detection are depicted in Fig. 2, both the PDSI and SPEI revealing two trend turnings in drought across various regions of the Afro-Eurasian continent during 1950–2018. These turnings are primarily concentrated in the eastern of Eurasian, Europe and Sahel, highlighting the dynamic nature of drought variability in these regions. These areas also align with hotspots of drought research identified in previous studies (Bakke et al., 2023; Popova et al., 2015; Sun

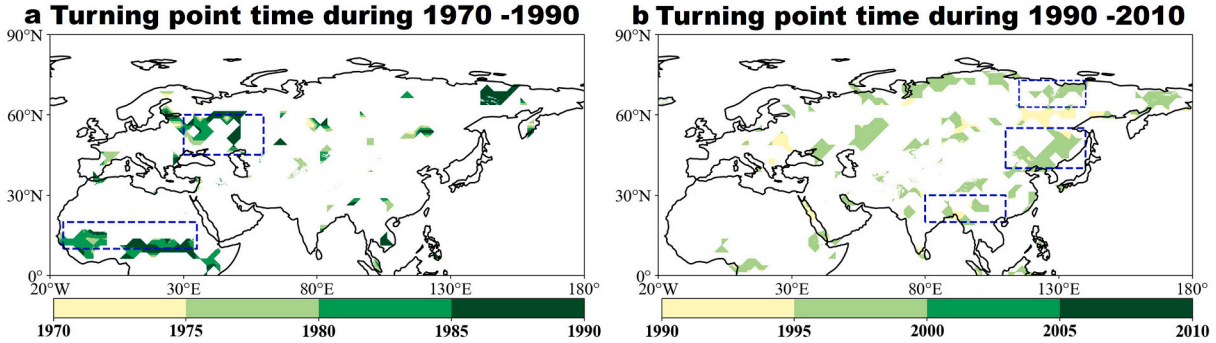

Fig. 4. (a) The timing of PDSI trend turnings across Afro-Eurasian continent that occurs during 1970–1990. (b) The timing of PDSI trend turnings across Afro-Eurasian continent that occurs during 1990–2010. Similar colors indicate concurrent turning. The blue box in it is the defined the region of Eastern Europe (45°N ~ 60°N, 30°E ~ 60°E), Sahel (10°N ~ 20°N, 15° W ~ 30°E), Russian Far East (63°N ~ 73°N, 115° E ~ 140°E), Northeast Asia (40°N ~ 55°N, 110°E ~ 140°E), and South Asia (20°N ~ 30°N, 80° E ~ 110°E). (For interpretation of the references to colour in this figure legend, the reader is referred to the web version of this article.)

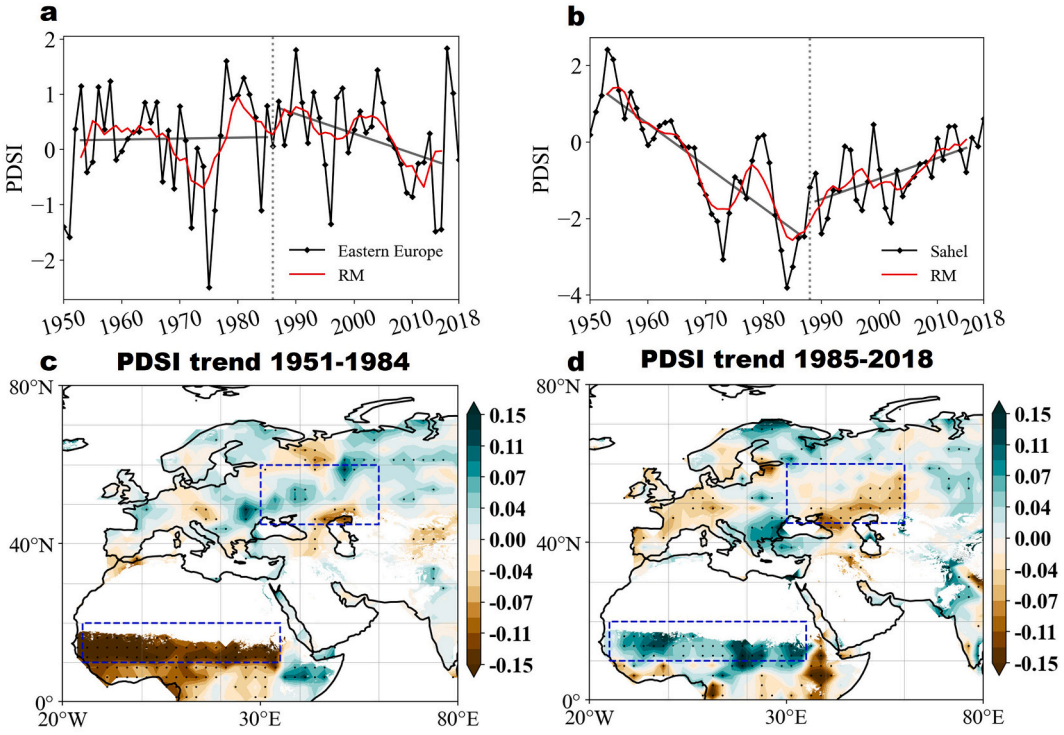

Fig. 5. Time series of the annual average of the PDSI in (a) Eastern Europe (b) Sahel from 1950 to 2018 (black dotted line) with their detection results (grey solid line). Note: The red line represents the 7-year sliding average time series of the PDSI; (c) Trend of the PDSI from 1951 to 1984 (yr^{-1}), (d) Trend of the PDSI from 1985 to 2018 (yr^{-1}). The blue box in it is the defined the region of Eastern Europe (45°N ~ 60°N, 30°E ~ 60°E) and Sahel (10°N ~ 20°N, 15° W ~ 30°E). Areas significant at the 95 % confidence level are denoted by dots. (For interpretation of the references to colour in this figure legend, the reader is referred to the web version of this article.)

et al., 2021; Ullah et al., 2023a; Yu et al., 2017). However, the types of trend turnings vary across different regions. Notably, wetting turnings are prevalent in Northeast Asia and Sahel (Fig. 3a and b), while drying turnings dominate Eastern Europe and South Asia (Fig. 3c and d), and both wet and dry turnings is present in the Russian Far East. The SPEI results are consistent with the PDSI particularly over Eastern Europe, Sahel, Russian Far East, Northeast Asia, and South Asia. Based on the results, five key regions are selected: Eastern Europe, the Sahel, the Russian Far East, Northeast Asia, and South Asia. These regions not only exhibit high drought trend turning frequencies, but also display temporally concurrent drought trend turnings: Eastern Europe and the Sahel PDSI experienced a concurrent trend turning during 1970–1990, while Eastern Eurasia, including the Russian Far East, Northeast Asia and South Asia experienced a concurrent trend turning during 1990–2010 (Fig. 4). Therefore, further analysis of PDSI trend turnings and their concurrence within these regions is warranted.

3.2. *Concurrent trend turnings in different regions of Afro-Eurasian drought severity*

Based on the results of the frequency of drought trend turnings described above. We calculate regional average PDSI time series for the five key regions across Afro-Eurasian (Eastern Europe, Sahel, Russian Far East, Northeast Asia, and South Asia) from 1950 to 2018. The RSD *t*-test is individually applied to the five regional average drought index time series. We find concurrent trend turnings in these regions at some

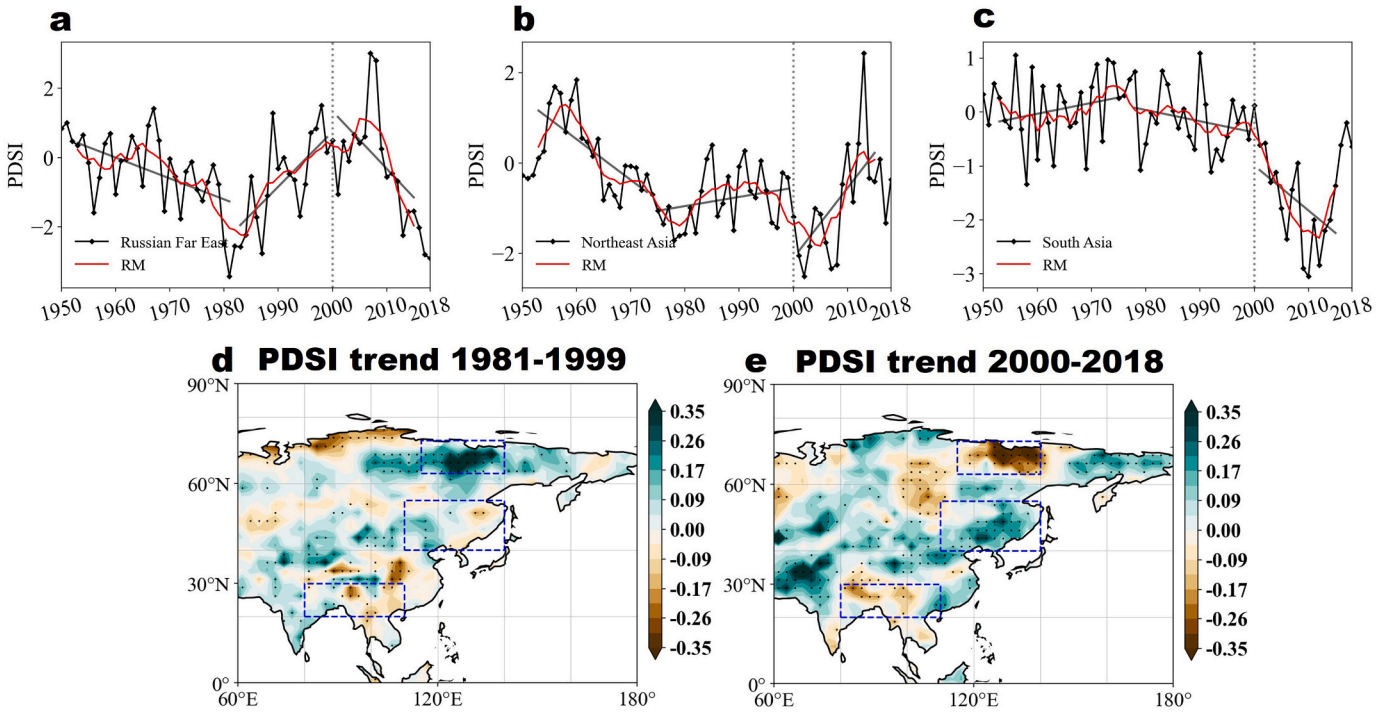

Fig. 6. Time series of the annual average of the PDSI in (a) Russian Far East (b) Northeast Asia (c) South Asia from 1950 to 2018 (black dotted line) with their detection results (grey solid line). Note: The red line represents the 7-year sliding average time series of the PDSI; (d) Trend of the PDSI from 1981 to 1999 (yr^{-1}), (e) Trend of the PDSI from 2000 to 2018 (yr^{-1}). The blue box in it is the defined the region of Russian Far East (63°N ~ 73°N, 115°E ~ 140°E), Northeast Asia (40°N ~ 55°N, 110°E ~ 140°E), and South Asia (20°N ~ 30°N, 80°E ~ 110°E). Areas significant at the 95 % confidence level are denoted by dots. (For interpretation of the references to colour in this figure legend, the reader is referred to the web version of this article.)

point in time. As shown in Fig. 5a-b, both Eastern Europe and the Sahel exhibit only one trend turning around 1985. However, these regions display contrasting trend turning patterns, forming a dipole structure. The Eastern Europe PDSI demonstrates an increasing trend until 1985, followed by a decreasing trend (drying trend turning). Conversely, the Sahel exhibits a trend turning from a decreasing to an increasing trend (wetting trend turning). Subsequently, drought severity intensifies in Eastern Europe, while it weakens in the African Sahel region. In eastern Eurasia (Russian Far East, Northeast Asia, and South Asia), all three regions experience two trend turnings, with the last one occurring around 2000 (Fig. 6a-c). These three regions also exhibit distinct trend turning patterns, forming a tripolar structure. The Russian Far East PDSI shows a trend turning from increasing to decreasing (drying trend turning). South Asia displays a stronger decreasing trend after 2000 compared to before (drying trend turning). Conversely, Northeast Asia experiences a stronger increasing trend after 2000 (wetting trend turning). Consequently, drought conditions improve in Northeast Asia, while drought severity intensifies in South Asia and the Russian Far East.

To corroborate the trend turnings, we compute the spatial long-term trend of PDSI in Afro-Eurasian around 1985 and 2000. Spatially, both the Eastern European and Sahel PDSI trends demonstrably change around 1985, exhibiting a dipole structure (Fig. 5c-d). Similarly, the spatial PDSI trends in the three regions of eastern Eurasia demonstrably change around 2000, displaying a tripole structure (Fig. 6d-e). We also evaluated the time series RSD t-test and spatial changing trends using SPEI data (Fig.S2 and S3), and the results align with the PDSI findings, confirming consistent trend turnings and spatial patterns.

To further demonstrate the concurrence of trend turnings in these different regions, we conduct a cross-tabulation analysis. Specifically, for the relationship between drought trend in Eastern Europe and Sahel, we categorize the trends of 72 Sahel grid points based on different trend scenarios in Eastern Europe (the drought trend in Eastern Europe shifted from a positive to a negative trend), including no significant trend, significant positive trend, and significant negative trend, and then conduct statistical analysis. Statistical analysis using a chi-square test reveals a significant association ($\chi^2 = 108.097$, $p < 0.01$) between drought trends in Eastern Europe and Sahel (Table 2). In other words, the transition from a positive to negative trend in Eastern Europe coincides with a shift from a significant negative to a significant positive trend in the Sahel. This remarkable concurrency underscores a strong teleconnection between their drought patterns. Similar analyses are also conducted for South Asia, Russian Far East, and Northeast Asia, revealing the drought trends in South Asia is significantly associated

Table 2
Statistics of different types of trends and Chi-Square Tests for Grid Points in the Sahel under Different Eastern Europe Drought Scenarios.

	No trend	Significant Positive	Significant Negative	Total
Eastern Europe +	8	1	63	72
Eastern Europe -	25	45	2	72
Total	33	46	65	144

The chi-square statistic is 108.0907. The *p*-value is 0.00001. The result is significant at $p < 0.01$.

Table 3
Statistics of different types of trends and Chi-Square Tests for Grid Points in the Russian Far East under Different South Asia Drought Scenarios.

	No trend	Significant Positive	Significant Negative	Total
South Asia -	15	24	1	40
South Asia –	14	1	25	40
Total	29	35	26	80

The chi-square statistic is 43.3483. The *p*-value is 0.00001. The result is significant at $p < 0.01$.

Table 4
Statistics of different types of trends and Chi-Square Tests for Grid Points in Northeast Asia under Different South Asian Drought Scenarios.

	No trend	Significant Positive	Significant Negative	Total
South Asia -	63	5	4	72
South Asia –	39	32	1	72
Total	102	37	5	144

The chi-square statistic is 27.1498. The p-value is 0.00001. The result is significant at $p < 0.01$.
Notes: + and - represent significant positive and significant negative trends, respectively; –- represents negative trends with trend values.

with those in Russian Far East ($\chi^2 = 43.3483$, $p < 0.01$) and Northeast Asia ($\chi^2 = 27.1498$, $p < 0.01$) (Table 3 and Table 4). The transitions in drought trends (positive to negative in the Russian Far East and significantly positive to more positive in Northeast Asia) coincided with a shift from a significantly negative to a more negative trend in South Asia. This further strengthens the evidence for robust teleconnections among these geographically distinct regions.

These findings reveal the presence of concurrent drought trend turnings in numerous Afro-Eurasian regions, independent of data choice. Eastern Europe and the Sahel experience drought trend turnings around 1985, exhibiting dipole patterns: Eastern Europe turning from wet to dry, and the African Sahel turning from dry to wet. In Eastern Asia, the trend turning in drought patterns manifests as a tripolar structure. The Russian Far East, Northeast Asia, and South Asia experience trend turnings around 2000, with distinct patterns. Northeast Asia becomes wetter, the Russian Far East turns from wet to dry, and South Asia becomes drier. The underlying causes of these concurrent trend turnings and their contrasting nature remain unclear. Therefore, further analysis is required to elucidate the internal mechanisms driving these concurrent trend turnings in respective regions.

3.3. *Possible causes of concurrent trend turnings in Afro-Eurasian drought severity*

Anomalies in atmospheric circulation are primary drivers of drought, influencing both precipitation and evapotranspiration. Atmospheric circulation patterns impact the spatial distribution of precipitation and atmospheric heat transport, ultimately leading to decreased precipitation or increased evapotranspiration in specific regions, triggering drought conditions (Dai et al., 2018). Surface water availability (precipitation minus evapotranspiration, P-E) serves as a crucial indicator of climatic aridity and wetness. Deviations or limitations in surface water availability play a key role in drought formation and development, highlighting the close link between drought severity and P-E (Pokhrel et al., 2021). As shown in Fig. 7a-c, a dipole pattern of surface water availability trend emerges around the year 1985, with a significant decrease in Eastern Europe and an increase in the Sahel after 1985. We also conduct trend turning point detection on the P-E time series for both

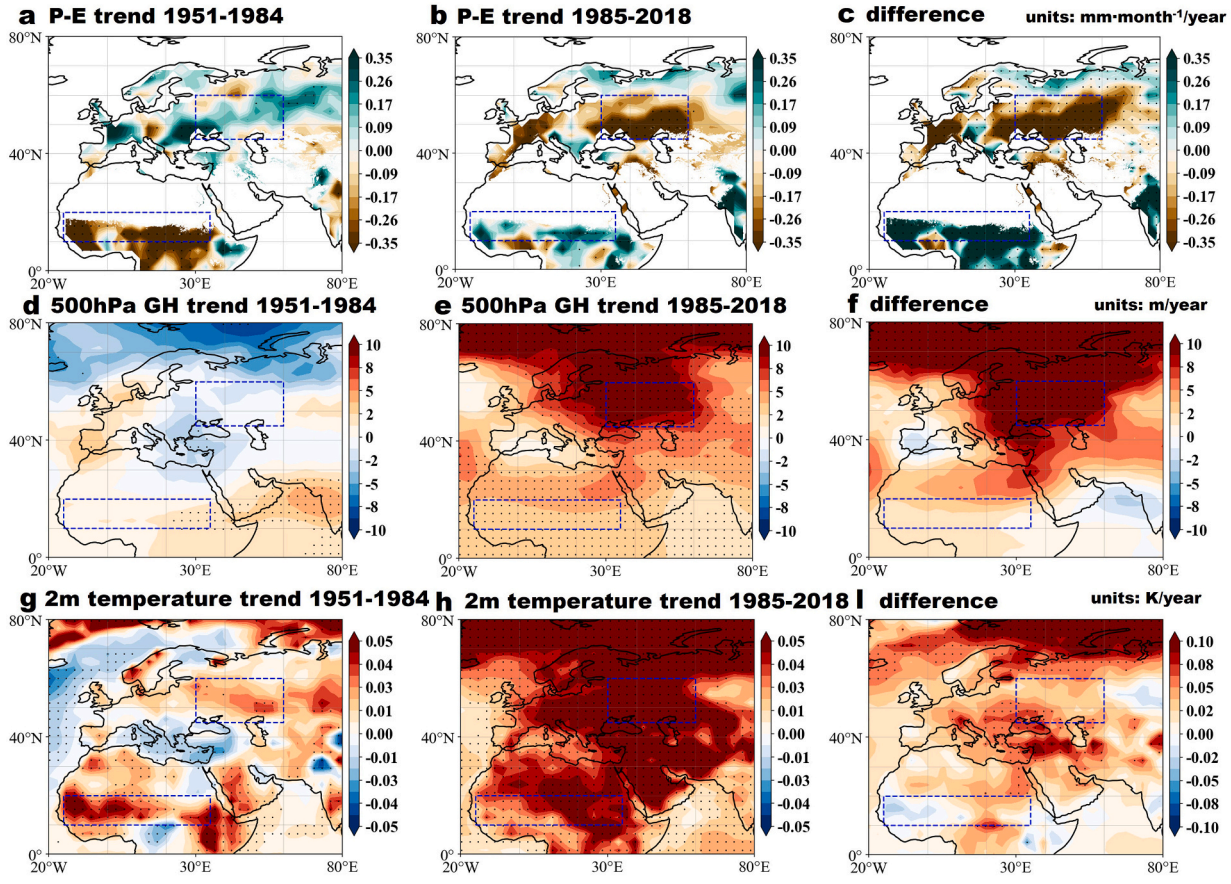

Fig. 7. Trend of the surface water availability (precipitation minus evaporation, P–E) from (a) 1951 to 1984 (mm·month^{-1}/ yr^{-1}) and (b) 1985 to 2018 (mm·month^{-1}/ yr^{-1}). (c) The difference between the surface water availability (precipitation minus evaporation, P–E) trend during 1985–2018 and 1951–1984. Trend of the 500 hPa geopotential height from (d) 1951 to 1984 (m/ yr^{-1}) and (e) 1985 to 2018 (m/ yr^{-1}). (f) The difference between the 500 hPa geopotential height trend during 1985–2018 and 1951–1984. Trend of the 2 m temperature from (g) 1951 to 1984 (K/ yr^{-1}) and (h) 1985 to 2018 (K/ yr^{-1}). (i) The difference between the 2 m temperature trend during 1985–2018 and 1951–1984. The blue box in it is the defined region of Eastern Europe (45°N ~ 60°N, 30°E ~ 60°E) and Sahel (10°N ~ 20°N, 15° W ~ 30°E). Areas significant at the 95 % confidence level are denoted by dots. (For interpretation of the references to colour in this figure legend, the reader is referred to the web version of this article.)

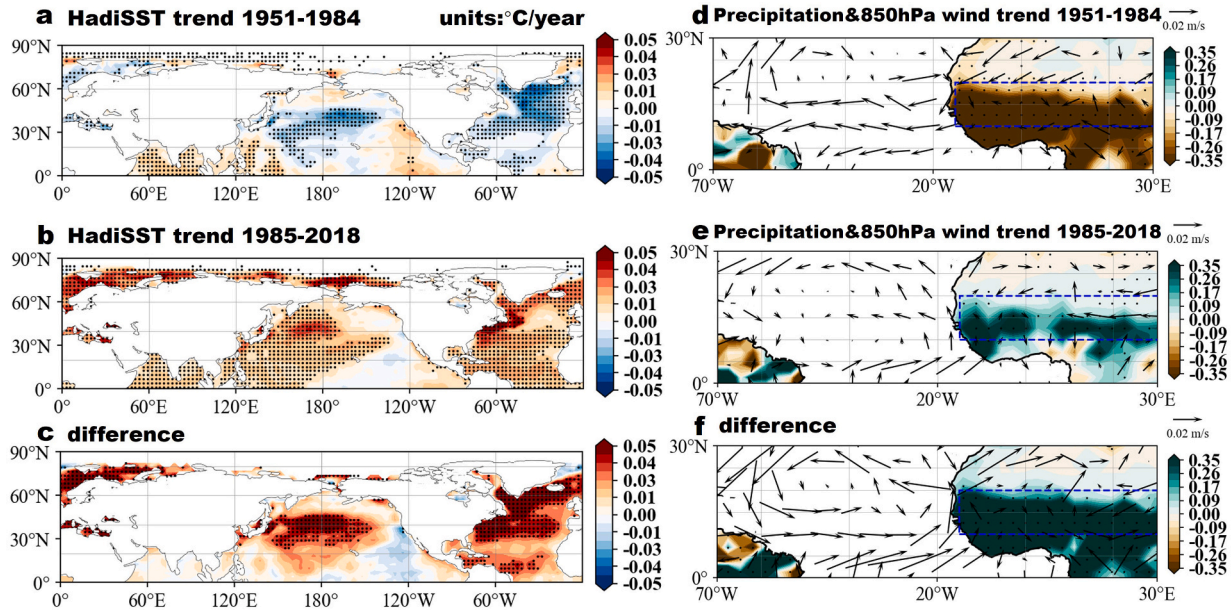

Fig. 8. Trend of the SST from (a) 1951 to 1984 (°C/ yr^{-1}) and (b) 1985 to 2018 (°C/ yr^{-1}). (c) The difference between the SST trend during 1985–2018 and 1951–1984. Trend of the precipitation and 850 hPa wind (vector) from (d) 1951 to 1984 (mm·$month^{-1}$/ yr^{-1}) and (e) 1985 to 2018 (mm·$month^{-1}$/ yr^{-1}). (f) The difference between the precipitation and 850 hPa wind (vector) trend during 1985–2018 and 1951–1984. The blue box in it is the defined region of Sahel (10°N ~ 20°N, 15° W ~ 30°E). Areas significant at the 95 % confidence level are denoted by dots. (For interpretation of the references to colour in this figure legend, the reader is referred to the web version of this article.)

regions from 1950 to 2018. As shown in Fig. S4a-b, the P-E time series for Eastern Europe and the Sahel indicate a trend turning point around 1985. In Eastern Europe, the P-E time series shows a declining trend post-1985, consistent with PDSI, indicating reduced surface water availability and intensified drought severity. Conversely, in the Sahel, the P-E time series shows an increasing trend post-1985, also consistent with PDSI, indicating a recovery in surface water availability and reduced drought severity. By calculating the spatial trends of atmospheric circulation factors before and after 1985, it is found that the geopotential height and surface temperature over Eastern Europe have significantly increased since 1985 (Fig. 7d-i). Under the control of high pressure, the atmospheric thickness over Eastern Europe has increased and the temperature has risen, while the available surface water has decreased compared to before 1985. Consequently, therefore, the drought in Eastern Europe has intensified after 1985. The drought in the Africa Sahel region is primarily caused by insufficient precipitation (Epule et al., 2014). After 1985, the Sahel region experiences increased surface water availability and precipitation, coupled with decreased temperatures compared to the pre-1985 period (Fig. 7d-i). These changes are conducive to maintaining soil moisture, thus reducing drought severity to some extent.

Concurrent global drought events can be jointly driven by atmospheric teleconnections patterns and regional weather systems. Specifically, SST anomalies can influence atmospheric circulation patterns, thereby affecting the patterns and distribution of precipitation and temperature. Previous studies implicate global SST as a key driver of European drought (Ionita et al., 2012). As shown in Fig. 8a-c, the analysis of SST trends before and after 1985 shows that the SST in the Northern Hemisphere has warmed significantly since 1985, exerting a heating effect on the atmosphere. The significant increase in geopotential height and surface temperature in Europe has led to a decrease in precipitation. At the same time, the temperature rise also triggered stronger evaporation, leading to a decrease in water availability on the land surface. This forms a positive feedback process, ultimately exacerbating the severity of drought conditions. The interannual variation of precipitation in Sahel is mainly driven by SST (Mohino et al., 2011). As shown in Fig. 8d-f, after 1985, there is a significant warming of the northern hemisphere SST, an increase in the temperature difference between the northern and southern hemispheres, leading to a strengthening of the tropical cross-equatorial airflow. The cross-equatorial airflow is conducive to transporting warm and humid airflow to the Sahel region, bringing abundant water vapor, and increasing precipitation in the Sahel, thus alleviating the drought severity to some extent.

Fig. 9a-f reveals a tripole trend change in surface water availability and precipitation over East Asia around 2000. Notably, Northeast Asia exhibits a significant increase trend, contrasting with decrease trend in Russian Far East and South Asia. Similarly, the P-E time series for the Russian Far East, Northeast Asia, and South Asia exhibit trend turning points around 2000, consistent with PDSI. As shown in Fig. S4c-e, Northeast Asia's P-E time series indicates an increasing trend post-2000, reflecting enhanced surface water availability and reduced drought severity. Conversely, the Russian Far East and South Asia show decreasing trends post-2000, also consistent with PDSI, indicating decreased surface water availability and intensified drought severity. This tripole structure also extends to 500 hPa geopotential height (Fig. 9g-i). A significant increase in geopotential height is conducive to air subsidence, which suppresses the upward movement and condensation of water vapor, resulting in a decrease in precipitation. Conversely, a significant decrease in geopotential height facilitates the enhancement of low-level convergence, which in turn promotes precipitation. Thus, the tripolar structure manifests in PDSI, signifying dryness in the Russian Far East and South Asia and increased wetness in Northeast Asia. These findings highlight the complex interplay between atmospheric circulation and climate variables in East Asia. The observed tri-polar structure underscores regional variability in climate change impacts and emphasizes the need for tailored adaptation strategies.

Decadal East Asian precipitation variations strongly associate with North Pacific Ocean SST (Zhang et al., 2018). Fig. 10 illustrates significant SST changes and a post-2000 meridional tri-polar pattern in the North Pacific. We examine ENSO, the dominant SST mode in the Pacific Ocean, using the Nino3.4 time series but reveals no significant trend turnings sign during the analysis period (Fig. S5). Beyond ENSO, the NPGO is recognized as a significant mode in the North Pacific. Previous

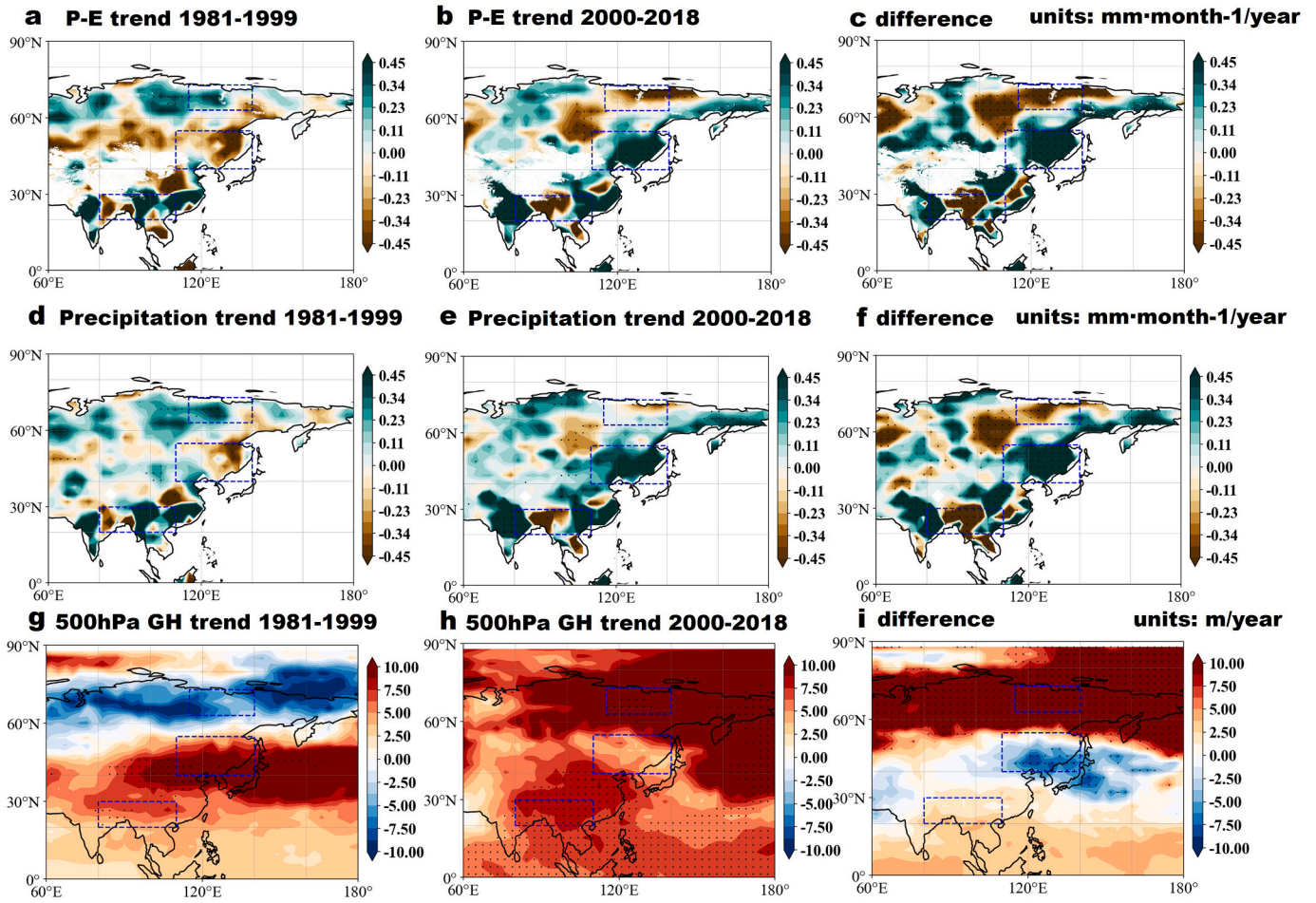

Fig. 9. Trend of the surface water availability (precipitation minus evaporation, P–E) from (a) 1981 to 1999 (mm·month^{-1}/ yr^{-1}) and (b) 2000 to 2018 (mm·month^{-1}/ yr^{-1}). (c) The difference between the surface water availability (precipitation minus evaporation, P–E) trend during 2000–2018 and 1981–1999. Trend of the precipitation from (d) 1981 to 1999 (mm·month^{-1}/ yr^{-1}) and (e) 2000 to 2018 (mm·month^{-1}/ yr^{-1}). (f) The difference between the precipitation trend during 2000–2018 and 1981–1999. Trend of the 500 hPa geopotential height from (g) 1981 to 1999 (m/ yr^{-1}) and (h) 2000 to 2018 (m/ yr^{-1}). (i) The difference between the 500 hPa geopotential height trend during 2000–2018 and 1981–1999. The blue box in it is the defined the region of Russian Far East (63°N ~ 73°N, 115°E ~ 140°E), Northeast Asia (40°N ~ 55°N, 110°E ~ 140°E) and South Asia (20°N ~ 30°N, 80°E ~ 110°E). Areas significant at the 95 % confidence level are denoted by dots. (For interpretation of the references to colour in this figure legend, the reader is referred to the web version of this article.)

studies have shown that the variability of the NPGO has intensified since the 1990s, significantly influencing climate systems across the North Pacific region and remote areas. (Cummins and Freeland, 2007; Kai and Congwen, 2015). Then, we regress the NPGO index to the 500 hPa geopotential height field and find a strong north-south dipole response over the North Pacific Ocean, as well as a strong negative anomalous potential height response over East Asia (Fig.S6). Notably, the NPGO shifts to positive phase after 2000. We further calculate the interdecadal potential geostrophic height difference between the positive and negative phases of the NPGO. Fig. 11 shows the 500 hPa geopotential height difference between the two phases (positive minus negative). Overall, during the NPGO positive phase years, the geopotential height is lower over the East Asian mid-latitudes and higher over the Russian Far East and South Asia. The centers of the high-pressure anomalies are associated with less precipitation, while the centers of the low-pressure anomalies are associated with more precipitation. Therefore, we suggest NPGO phase transition-induced geopotential height and precipitation anomalies may have contributed to the tri-polar drought trend turning in East Asia around 2000.

In summary, this study explores how large-scale SST anomalies can remotely influence regional drought patterns and trigger concurrent drought trend turnings through atmospheric teleconnections and positive feedback processes. Our investigation focuses on elucidating the large-scale drivers of concurrent trend turnings of drought across distinct Afro-Eurasian regions. Our study suggests that hemisphere-scale ocean warming causing uplift of geopotential height and changes in cross-equatorial airflow induce decreasing in P-E in Eastern Europe and increase in P-E in Sahel, resulting in a dipole type of drought trend turning in Eastern Europe and Sahel in the western of Afro-Eurasian continent. This indicates an intensification of drought trends in Eastern Europe and a weakening of drought trends in the Sahel. Simultaneously, the shift of the phase of large-scale ocean-atmosphere coupled modes in the Pacific leads to the formation of a tripole circulation pattern in Eastern Eurasia, inducing decreasing in P-E in Russian Far East and South Asia, and increasing in Northeast Asia. This tripole pattern of atmospheric circulation is linked to a corresponding tripole pattern of drought trend turning in the region.

4. Discussion

Our analysis reveals distinct patterns of drought trend turnings across Afro-Eurasian. The Sahel and Northeast Asia exhibit a wetting trend turning, characterized by a transition towards wetter conditions. Conversely, Eastern Europe, South Asia, and the Russian Far East experience a drying trend turning, indicating a shift towards drier conditions. These findings align well with existing research. For

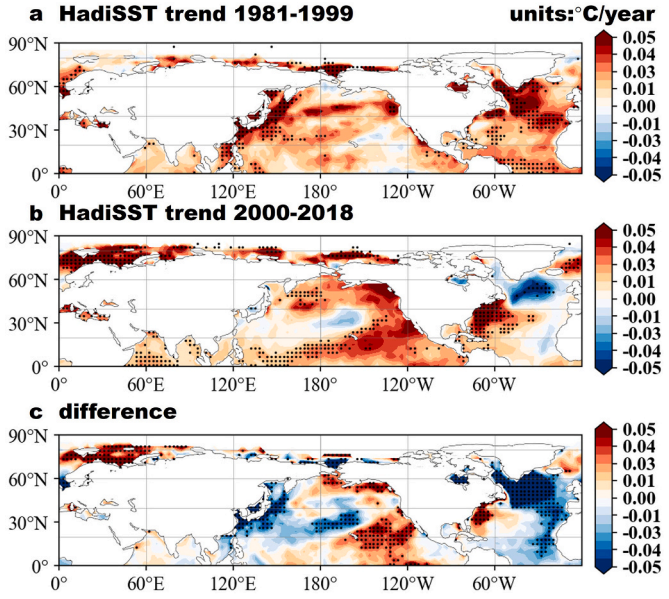

Fig. 10. Trend of the SST from (a) 1981 to 1999 (°C/ yr^{-1}) and (b) 2000 to 2018 (°C/ yr^{-1}). (c) The difference between the SST trend during 2000–2018 and 1981–1999. Areas significant at the 95 % confidence level are denoted by dots.

instance: Satellite observations have revealed some recovery from drought severity in Sahel (Chen et al., 2020). Eastern Europe is experiencing a more remarkable drying trend than before(Spinoni et al., 2017). Water resources have been under strain in northern Siberia and South Asia in recent decades (Churakova Sidorova et al., 2020; Sidorova et al., 2009; Ullah et al., 2022), while precipitation has increased in Northeast Asia (Li et al., 2022; Si et al., 2021; Ullah et al., 2022). Notably, despite the recent "wetting" trends observed in the Sahel and Northeast Asia over the past decade, which may temporarily facilitate vegetation recovery and enhance local ecosystem health, their overall moisture anomalies remain significantly negative relative to historical baselines, indicating persistent water scarcity. This underscores the enduring drought risks in these regions, necessitating ongoing enhancement of drought monitoring and management strategies. Additionally, intensifying drought trends in Eastern Europe and South Asia, as evidenced by the frequent occurrence of drought and extreme heat events in recent years, pose a significant threat to regional ecosystems and agricultural productivity. These trends could lead to a cascade of detrimental consequences, including: vegetation loss, erosion, biodiversity decline, ecosystem degradation, and crop failures. Therefore, these regions require special attention to strengthen water resource management and proactively mitigate social, ecological, and agricultural risks.

Overall, our analysis reveals the spatio-temporal characteristics of drought trend turnings across the Afro-Eurasian continent and emphasizes the role of large-scale factors in linking the drought trend turnings between different regions. These findings highlight that, in addition to local driving factors, future drought studies need to pay more attention to large-scale factors such as interdecadal SST. By identifying the turning points in drought trends and revealing the connections between shifts in drought trends across various regions, our research contributes to forecasting impending drought incidents within these zones, thereby augmenting the efficacy and synergism of drought disaster mitigation efforts on a broad regional basis. Concurrently, we also highlight some considerations and limitations of this study. Firstly, the RSD method offers distinct advantages for detecting interdecadal trend changes in time series (Ghaderpour et al., 2024). This study employed the RSD approach to specifically investigate the evolution of interdecadal drought trends. However, drought is a multifaceted phenomenon that manifests across various temporal scales. The current study does not delve into short-term drought variations, such as abrupt events or seasonal fluctuations. Future research will focus on the spatiotemporal characteristics of short-term drought trend changes. Furthermore, local factors, including land use and irrigation practices, can significantly influence local climate conditions. These local factors will be incorporated into future studies to provide a more comprehensive understanding of drought dynamics.

Our study identifies the NPGO as a significant factor in the interregional linkage of drought trend turnings in eastern Eurasia. Recent studies reveal a significant upward trend in NPGO variability since 1990, which is projected to further increase under the backdrop of global warming (Ji et al., 2024). Therefore, it is very likely that NPGO will have a more significant effect on the East Asian circulation in the future, providing new insights into the prediction of dry and wet conditions in East Asia. Moreover, since the late 1990s, a hiatus in the upward trend of global average temperatures has been observed, a phenomenon known as the Hiatus (Fyfe et al., 2016). Hiatus may lead to changes in global precipitation patterns, which in turn could affect the occurrence and intensity of regional droughts. Studies have shown that the Hiatus has a significant impact on global drought changes (Kong et al., 2019; Wang et al., 2016). For example, droughts in the United States are more frequent during the Hiatus (Mazdiyasni and AghaKouchak, 2015). Therefore, the Hiatus may be an important factor to consider when assessing drought trend turnings.

In addition to natural variability, external forcings such as global warming and aerosols may also contribute to trend turnings in drought. Since the industrial revolution, greenhouse gas emissions have intensified the greenhouse effect, leading to increased potential evapotranspiration and a deficit in water input, resulting in drought (Dai et al.,

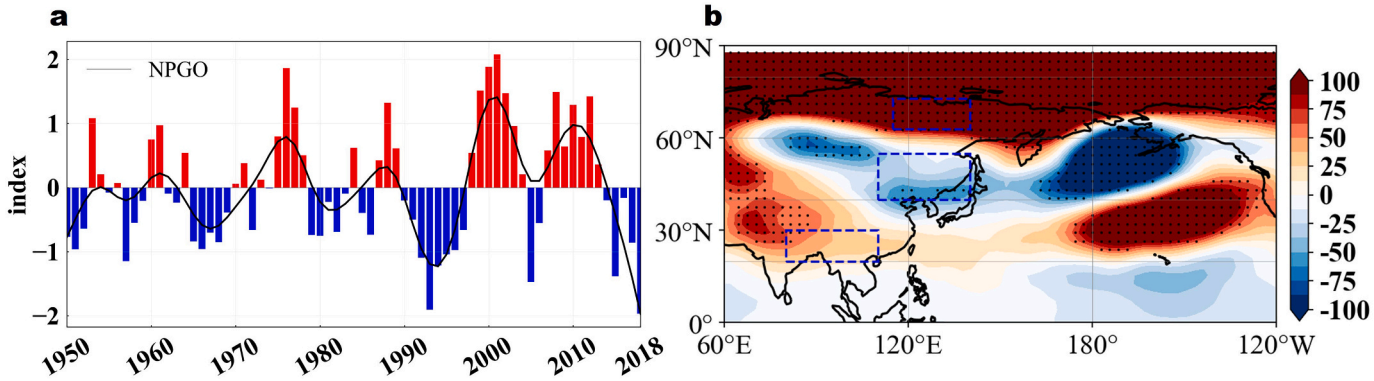

Fig. 11. (a) Time series of NPGO index and 10-year filtered NPGO index (black solid line). (b) Composite differences between positive and negative interdecadal NPGO periods of 500 hPa geopotential height. Areas significant at the 95 % confidence level are denoted by dots.

2018). Climate change has exacerbated drought characteristics, including frequency and severity (Kim et al., 2020). Coupled simulations under various greenhouse gas emission scenarios indicate a substantial decrease in soil moisture in regions like Europe and Southeast Asia (Balting et al., 2021). Since the 1950s, anthropogenic aerosol emissions have increased significantly worldwide. Studies have shown that aerosols can delay and suppress large-scale precipitation, leading to a weakening of the water cycle (Wang et al., 2022). The direct cooling effect caused by the increase in anthropogenic aerosols not only causes local circulation changes and intensifies drought, but can also further regulate the water cycle through atmospheric teleconnections, affecting drought in areas far from the aerosol source region (Yeh et al., 2015; Zhang et al., 2017). It is necessary to further use models to distinguish the influence of global warming and aerosols on drought trend turnings in the future. The primary focus of this study is on the linkages and concurrence between regional drought trend turnings, and the RSD-*t*-test method can statistically identify the most significant turning points and more suitable for studying concurrent drought trend turnings across different regions. In future studies, we will further explore the temporal evolution of drought patterns using other change-point detection methods (Jandhyala et al., 2013).

5. Conclusion

Drought in Afro-Eurasian has received widespread attention. Previous studies have mainly focused on the long-term trends of drought, but the frequency and spatial distribution of trend turnings and the internal linkages between trend turnings in different regions are remain largely unexplored. In this study, we apply a recently proposed method for detecting the frequency of climate trend turning, the RSD-t-test, to the PDSI of the Afro-Eurasian to obtain the types and frequency-space distribution of drought trend turnings in Afro-Eurasian. The results show that most of the PDSI in most areas of Afro-Eurasian experience two trend turnings during 1950–2018. Around 1985, a dipole drought trend turning emerged in the western of Afro-Eurasian, with Eastern Europe experiencing a drying trend turning with decreased P-E and intensified drought, while the Sahel exhibited a wetting trend turning with increased P-E and mitigated drought. Around 2000, a tripole drought trend turning emerged in the eastern of Afro-Eurasian, with the Russian Far East and South Asia experiencing drying trend turning with reduced P-E and intensified drought, while Northeast Asia showed a wetting trend turning with increased P-E and mitigated drought. Large-scale SST as a key driver in the linkage of inter-regional concurrent trend turnings. Hemisphere-scale ocean warming elevates geopotential height and alters cross-equatorial airflow, decreasing P-E in Eastern Europe and increasing P-E in Sahel, forming a dipole drought trend pattern with intensifying drought in Eastern Europe and weakening in Sahel. The shifts in NPGO modes create a tripole atmospheric circulation pattern in the eastern of Eurasia, decreasing P-E in the Russian Far East and South Asia while increasing P-E in Northeast Asia, resulting in a tripole drought trend pattern with intensifying drought in Russian Far East, South Asia, and weakening in Northeast Asia.

CRediT authorship contribution statement

Wei Lou: Writing – review & editing, Writing – original draft, Formal analysis. **Cheng Sun:** Writing – review & editing, Formal analysis, Conceptualization. **Bin Zuo:** Writing – review & editing, Data curation.

Declaration of competing interest

The authors declare that they have no known competing financial interests or personal relationships that could have appeared to influence the work reported in this paper.

Data availability

The original observational data are publicly available. All data sources are mentioned in the Data and Methods section. The source codes for the analysis of this study are available from the corresponding author upon reasonable request.

Acknowledgments

This research is jointly supported by the National Key Research and Development Program of China (2020YFA0608401), and the National Natural Science Foundation of China (42375025).

Appendix A. Supplementary data

Supplementary data to this article can be found online at https://doi.org/10.1016/j.gloplacha.2024.104628.

References

Ault, T.R., 2020. On the essentials of drought in a changing climate. Science 368 (6488), 256–260.
Ayugi, B., et al., 2022. Review of Meteorological Drought in Africa: Historical Trends, Impacts, Mitigation measures, and prospects. Pure Appl. Geophys. 179 (4), 1365–1386.
Bakke, S.J., Ionita, M., Tallaksen, L.M., 2023. Recent European drying and its link to prevailing large-scale atmospheric patterns. Sci. Rep. 13 (1), 21921.
Balting, D.F., AghaKouchak, A., Lohmann, G., Ionita, M., 2021. Northern Hemisphere drought risk in a warming climate. Npj Clim. Atmos. Sci. 4 (1), 61.
Beguería, S., Serrano, S.M.V., Reig-Gracia, F., Garcés, B.L., 2023. SPEIbase v.2.8 [Dataset].
Biasutti, M., Giannini, A., 2006. Robust Sahel drying in response to late 20th century forcings. Geophys. Res. Lett. 33 (11).
Burke, E.J., Brown, S.J., Christidis, N., 2006. Modeling the recent Evolution of Global Drought and Projections for the Twenty-first Century with the Hadley Centre climate Model. J. Hydrometeorol. 7 (5), 1113–1125.
Byrne, M.P., O'Gorman, P.A., 2015. The Response of Precipitation Minus Evapotranspiration to climate Warming: why the "Wet-Get-Wetter, Dry-Get-Drier" Scaling does not hold over Land. J. Clim. 28 (20), 8078–8092.
Cao, D., et al., 2022. Projected increases in global terrestrial net primary productivity loss caused by drought under climate change. Earth's Future 10 (7) e2022EF002681.
Chen, H., Sun, J., 2019. Increased population exposure to extreme droughts in China due to 0.5 °C of additional warming. Environ. Res. Lett. 14 (6), 064011.
Chen, G., et al., 2012. Drought in the Southern United States over the 20th century: variability and its impacts on terrestrial ecosystem productivity and carbon storage. Clim. Chang. 114 (2), 379–397.
Chen, J., et al., 2018. Population exposure to droughts in China under the 1.5 °C global warming target. Earth Syst. Dynam. 9 (3), 1097–1106.
Chen, T., et al., 2020. The greening and wetting of the Sahel Have Leveled off since about 1999 in relation to SST. Remote Sens. 12 (17), 2723.
Chen, X., et al., 2022. Projected dry/wet regimes in China using SPEI under four SSP-RCPs based on statistically downscaled CMIP6 data. Int. J. Climatol. 42 (16), 9357–9384.
Chen, H., Wang, S., Zhu, J., Wang, D., 2023. Projected changes in the Pattern of Spatially compounding Drought and Pluvial events over Eastern China under a Warming climate. Earth's Future 11 (5) e2022EF003397.
Chiang, F., Mazdiyasni, O., AghaKouchak, A., 2021. Evidence of anthropogenic impacts on global drought frequency, duration, and intensity. Nat. Commun. 12 (1), 2754.
Churakova Sidorova, O.V., et al., 2020. Recent atmospheric drying in Siberia is not unprecedented over the last 1,500 years. Sci. Rep. 10 (1), 15024.
Cummins, P.F., Freeland, H.J., 2007. Variability of the North Pacific current and its bifurcation. Prog. Oceanogr. 75 (2), 253–265.
Dai, A., 2011. Characteristics and trends in various forms of the Palmer Drought Severity Index during 1900–2008. J. Geophys. Res. Atmos. 116 (D12).
Dai, A., 2013. Increasing drought under global warming in observations and models. Nat. Clim. Chang. 3 (1), 52–58.
Dai, A., 2017. Dai Global Palmer Drought Severity Index (PDSI). Research Data Archive at the National Center for Atmospheric Research. Computational and Information Systems Laboratory, Boulder, CO.
Dai, A., Zhao, T., Chen, J., 2018. Climate Change and Drought: a Precipitation and Evaporation Perspective. Curr. Clim. Chang. Rep. 4 (3), 301–312.
Di Lorenzo, E., et al., 2008. North Pacific Gyre Oscillation links ocean climate and ecosystem change. Geophys. Res. Lett. 35 (8).
Du, Y., Zhang, J., Zhao, S., Chen, H., 2020. Impact of the Eastward Shift in the Negative-phase NAO on Extreme Drought over Northern China in Summer. J. Geophys. Res. Atmos. 125 (16) e2019JD032019.
El Kenawy, A.M., et al., 2020. Evidence for intensification of meteorological droughts in Oman over the past four decades. Atmos. Res. 246, 105126.
Epule, E.T., Peng, C., Lepage, L., Chen, Z., 2014. The causes, effects and challenges of Sahelian droughts: a critical review. Reg. Environ. Chang. 14 (1), 145–156.

Fyfe, J.C., et al., 2016. Making sense of the early-2000s warming slowdown. Nat. Clim. Chang. 6 (3), 224–228.
Gebremeskel Haile, G., et al., 2019. Droughts in East Africa: Causes, impacts and resilience. Earth Sci. Rev. 193, 146–161.
Ghaderpour, E., Antonielli, B., Bozzano, F., Scarascia Mugnozza, G., Mazzanti, P., 2024. A fast and robust method for detecting trend turning points in InSAR displacement time series. Comput. Geosci. 185, 105546.
Guttman, N.B., 1998. Comparing the PALMER drought index and the STANDARDIZED precipitation INDEX1. JAWRA J. Am. W. Resour. Assoc. 34 (1), 113–121.
Hagos, S.M., Cook, K.H., 2008. Ocean Warming and Late-Twentieth-Century Sahel Drought and Recovery. J. Clim. 21 (15), 3797–3814.
Han, J., Singh, V.P., 2023. A review of widely used drought indices and the challenges of drought assessment under climate change. Environ. Monit. Assess. 195 (12), 1438.
He, B., et al., 2021. Spatio-temporal evolution and non-stationary characteristics of meteorological drought in inland arid areas. Ecol. Indic. 126, 107644.
Herrera-Estrada, J.E., Satoh, Y., Sheffield, J., 2017. Spatiotemporal dynamics of global drought. Geophys. Res. Lett. 44 (5), 2254–2263.
Ionita, M., Lohmann, G., Rimbu, N., Chelcea, S., Dima, M., 2012. Interannual to decadal summer drought variability over Europe and its relationship to global sea surface temperature. Clim. Dyn. 38 (1), 363–377.
Jandhyala, V., Fotopoulos, S., MacNeill, I., Liu, P., 2013. Inference for single and multiple change-points in time series. J. Time Ser. Anal. 34 (4), 423–446.
Ji, K., et al., 2024. Enhanced North Pacific Victoria mode in a warming climate. Npj Clim. Atmos. Sci. 7 (1), 49.
Kai, L.I.U., Congwen, Z.H.U., 2015. Regime Shift of Winter North Pacific Sea Surface Temperature after 1990 and its possible Causes. Chin. J. Atmos. Sci. 39 (5), 926–940.
Karl, T.R., Knight, R.W., Baker, B., 2000. The record breaking global temperatures of 1997 and 1998: evidence for an increase in the rate of global warming? Geophys. Res. Lett. 27 (5), 719–722.
Kim, J.-B., So, J.-M., Bae, D.-H., 2020. Global Warming Impacts on Severe Drought Characteristics in Asia Monsoon Region. Water 12, 1360.
King, A.D., Pitman, A.J., Henley, B.J., Ukkola, A.M., Brown, J.R., 2020. The role of climate variability in Australian drought. Nat. Clim. Chang. 10 (3), 177–179.
Kong, X., et al., 2019. Decadal Change in Soil Moisture over East Asia in Response to a Decade-Long Warming Hiatus. J. Geophys. Res. Atmos. 124 (15), 8619–8630.
Leeper, R.D., et al., 2022. Characterizing U.S. drought over the past 20 years using the U. S. drought monitor. Int. J. Climatol. 42 (12), 6616–6630.
Leng, G., Hall, J., 2019. Crop yield sensitivity of global major agricultural countries to droughts and the projected changes in the future. Sci. Total Environ. 654, 811–821.
Li, J., Zhao, Y., Chen, D., Kang, Y., Wang, H., 2022. Future precipitation changes in three key sub-regions of East Asia: the roles of thermodynamics and dynamics. Clim. Dyn. 59 (5), 1377–1398.
Liu, Y., et al., 2023. The patterns, magnitude, and drivers of unprecedented 2022 mega-drought in the Yangtze River Basin, China. Environ. Res. Lett. 18 (11), 114006.
Mazdiyasni, O., AghaKouchak, A., 2015. Substantial increase in concurrent droughts and heatwaves in the United States. Proc. Natl. Acad. Sci. 112 (37), 11484–11489.
Méndez, M., Magaña, V., 2010. Regional Aspects of Prolonged Meteorological Droughts over Mexico and Central America. J. Clim. 23 (5), 1175–1188.
Mohino, E., Janicot, S., Bader, J., 2011. Sahel rainfall and decadal to multi-decadal sea surface temperature variability. Clim. Dyn. 37 (3), 419–440.
Mondal, S., Mishra, K., Leung, R., Cook, B., 2023. Global droughts connected by linkages between drought hubs. Nat. Commun. 14 (1), 144.
Motha, R.P., 2011. The Impact of Extreme Weather events on Agriculture in the United States. In: Attri, S.D., Rathore, L.S., Sivakumar, M.V.K., Dash, S.K. (Eds.), Challenges and Opportunities in Agrometeorology. Springer, Berlin Heidelberg, Berlin, Heidelberg, pp. 397–407.
Mukherjee, S., Mishra, A.K., 2021. Increase in compound Drought and Heatwaves in a Warming World. Geophys. Res. Lett. 48 (1) e2020GL090617.
Nasrollahi, N., et al., 2015. How well do CMIP5 climate simulations replicate historical trends and patterns of meteorological droughts? Water Resour. Res. 51 (4), 2847–2864.
Overpeck, J.T., 2013. The challenge of hot drought. Nature 503 (7476), 350–351.
Phan-Van, T., et al., 2022. Drought over Southeast Asia and its Association with Large-Scale Drivers. J. Clim. 35 (15), 4959–4978.
Pokhrel, Y., et al., 2021. Global terrestrial water storage and drought severity under climate change. Nat. Clim. Chang. 11 (3), 226–233.
Popova, V.V., Zolotokrylin, A.N., Cherenkova, E.A., Titkova, T.B., 2015. Droughts in North Eurasia and climate Warming: Regional changes and Consequences. In: Haruyama, S., Shiraiwa, T. (Eds.), Environmental Change and the Social Response in the Amur River Basin. Springer Japan, Tokyo, pp. 129–148.
Saleem, F., Zeng, X., Hina, S., Omer, A., 2021. Regional changes in extreme temperature records over Pakistan and their relation to Pacific variability. Atmos. Res. 250, 105407.
Saleem, F., et al., 2023. Population Exposure changes to mean and Extreme climate events over Pakistan and Associated Mechanisms. GeoHealth 7 (10) e2023GH000887.
Sharma, S., Mujumdar, P., 2017. Increasing frequency and spatial extent of concurrent meteorological droughts and heatwaves in India. Sci. Rep. 7 (1), 15582.
Si, D., Jiang, D., Hu, A., Lang, X., 2021. Variations in northeast Asian summer precipitation driven by the Atlantic multidecadal oscillation. Int. J. Climatol. 41 (3), 1682–1695.
Sidorova, O.V., et al., 2009. Do centennial tree-ring and stable isotope trends of Larix gmelinii (Rupr.) Rupr. Indicate increasing water shortage in the Siberian north? Oecologia 161 (4), 825–835.
Simpkins, G., 2018. Unprecedented Sahel drought. Nature. Climate Change 8 (8), 662.
Singh, J., Ashfaq, M., Skinner, C.B., Anderson, W.B., Singh, D., 2021. Amplified risk of spatially compounding droughts during co-occurrences of modes of natural ocean variability. Npj climate and Atmospheric. Science 4 (1), 7.
Singh, J., et al., 2022. Enhanced risk of concurrent regional droughts with increased ENSO variability and warming. Nat. Clim. Chang. 12 (2), 163–170.
Song, X., Song, Y., Chen, Y., 2020. Secular trend of global drought since 1950. Environ. Res. Lett. 15 (9), 094073.
Spinoni, J., Naumann, G., Carrao, H., Barbosa, P., Vogt, J., 2014. World drought frequency, duration, and severity for 1951–2010. Int. J. Climatol. 34 (8), 2792–2804.
Spinoni, J., Naumann, G., Vogt, J.V., 2017. Pan-European seasonal trends and recent changes of drought frequency and severity. Glob. Planet. Chang. 148, 113–130.
Sun, C., Zhu, L., Liu, Y., Hao, Z., Zhang, J., 2021. Changes in the drought condition over northern East Asia and the connections with extreme temperature and precipitation indices. Glob. Planet. Chang. 207, 103645.
Thanasis, V., Efthimia, B.-S., Dimitris, K., 2011. Estimation of linear trend onset in time series. Simul. Model. Pract. Theory 19 (5), 1384–1398.
Tomé, A.R., Miranda, P.M.A., 2004. Piecewise linear fitting and trend changing points of climate parameters. Geophys. Res. Lett. 31 (2).
Ullah, I., et al., 2022. Recent changes in drought events over south asia and their possible linkages with climatic and dynamic factors. Remote Sens. 14, 3219.
Ullah, I., et al., 2023a. Spatiotemporal characteristics of meteorological drought variability and trends (1981–2020) over South Asia and the associated large-scale circulation patterns. Clim. Dyn. 60 (7), 2261–2284.
Ullah, I., et al., 2023b. Recent and Projected Changes in Water Scarcity and Unprecedented Drought Events over Southern Pakistan, 11.
Vicente-Serrano, S.M., Beguería, S., López-Moreno, J.I., Angulo, M., El Kenawy, A., 2010. A New Global 0.5° Gridded Dataset (1901–2006) of a Multiscalar Drought Index: Comparison with Current Drought Index Datasets based on the Palmer Drought Severity Index. J. Hydrometeorol. 11 (4), 1033–1043.
Vogel, E., et al., 2019. The effects of climate extremes on global agricultural yields. Environ. Res. Lett. 14 (5), 054010.
Wang, L., Yuan, X., Xie, Z., Wu, P., Li, Y., 2016. Increasing flash droughts over China during the recent global warming hiatus. Sci. Rep. 6 (1), 30571.
Wang, Z., et al., 2017. Does drought in China show a significant decreasing trend from 1961 to 2009? Sci. Total Environ. 579, 314–324.
Wang, Z., et al., 2022. Roles of Atmospheric Aerosols in Extreme Meteorological events: a Systematic Review. Curr. Pollut. Rep. 8 (2), 177–188.
Xu, F., et al., 2024. Understanding climate change impacts on drought in China over the 21st century: a multi-model assessment from CMIP6. Npj Clim. Atmos. Sci. 7 (1), 32.
Yeh, S.-W., Park, R.J., Kim, M.J., Jeong, J.I., Song, C.-K., 2015. Effect of anthropogenic sulphate aerosol in China on the drought in the western-to-central US. Sci. Rep. 5 (1), 14305.
Yu, Y., et al., 2017. Observed positive vegetation-rainfall feedbacks in the Sahel dominated by a moisture recycling mechanism. Nat. Commun. 8 (1), 1873.
Zeng, Z., et al., 2023. Increased risk of flash droughts with raised concurrent hot and dry extremes under global warming. Npj Clim. Atmos. Sci. 6 (1), 134.
Zhang, L., Wu, P., Zhou, T., 2017. Aerosol forcing of extreme summer drought over North China. Environ. Res. Lett. 12 (3), 034020.
Zhang, Z., Sun, X., Yang, X.-Q., 2018. Understanding the Interdecadal Variability of East Asian Summer Monsoon Precipitation: Joint Influence of three Oceanic Signals. J. Clim. 31 (14), 5485–5506.
Zhao, H., et al., 2017. Timescale differences between SC-PDSI and SPEI for drought monitoring in China. Phys. Chem. Earth Parts A/B/C 102, 48–58.
Zuo, B., Li, J., Sun, C., Zhou, X., 2019. A new statistical method for detecting trend turning. Theor. Appl. Climatol. 138 (1), 201–213.